Ultranarrow-Band Wavelength-Selective Thermal Emission with Aperiodic Multilayered Metamaterials Designed by Bayesian Optimization

Atsushi Sakurai,[†,‡] Kyohei Yada,[§] Tetsushi Simomura,[§] Shenghong Ju,[‡,∥] Makoto Kashiwagi,[∥] Hideyuki Okada,[§] Tadaaki Nagao,[‡,∇] Koji Tsuda,[‡,⊥,#] and Junichiro Shiomi*[,‡,∥,#]

[†]Department of Mechanical and Production Engineering, Niigata University, 8050 Ikarashi 2-no-cho, Niigata 950-2181, Japan

[‡]National Institute for Materials Science, 1-2-1 Sengen, Tsukuba 305-0047, Japan

[§]Graduate School of Science and Technology, Niigata University, 8050 Ikarashi 2-no-cho, Niigata 950-2181, Japan

[∥]Department of Mechanical Engineering, The University of Tokyo, 7-3-1 Hongo, Bunkyo-ku, Tokyo 113-8654, Japan
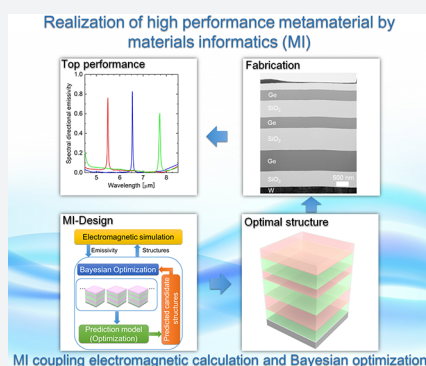
[⊥]Graduate School of Frontier Sciences, The University of Tokyo, 5-1-5 Kashiwa-no-ha, Kashiwa 277-8561, Japan

[#]RIKEN Center for Advanced Intelligence Project, 1-4-1 Nihombashi, Chuo-ku, Tokyo 103-0027, Japan

[∇]Department of Condensed Matter Physics Graduate School of Science, Hokkaido University, Kita-10 Nishi-8, Kita-ku, Sapporo 060-0810, Japan

S *Supporting Information*

ABSTRACT: We computationally designed an ultranarrow-band wavelength-selective thermal radiator via a materials informatics method alternating between Bayesian optimization and thermal electromagnetic field calculation. For a given target infrared wavelength, the optimal structure was efficiently identified from over 8 billion candidates of multilayers consisting of multiple components (Si, Ge, and SiO_2). The resulting optimized structure is an aperiodic multilayered metamaterial exhibiting high and sharp emissivity with a Q-factor of 273. The designed metamaterials were then fabricated, and reasonable experimental realization of the optimal performance was achieved with a Q-factor of 188, which is significantly higher than those of structures empirically designed and fabricated in the past. This is the first demonstration of the experimental realization of metamaterials designed by Bayesian optimization. The results facilitate the machine-learning-based design of metamaterials and advance our understanding of the narrow-band thermal emission mechanism of aperiodic multilayered metamaterials.

Realization of high performance metamaterial by materials informatics (MI)

INTRODUCTION

All materials emit or absorb thermal radiation. Therefore, in the exploration to utilize various thermal energy resources, tailoring thermal radiation plays a fundamentally important role.[1−3] While conventional thermal radiators typically exhibit broad-band, polarization-independent, and omnidirectional emission, the technology to control thermal radiation is rapidly progressing with the development of the fields of nanophotonics and metamaterials. Electromagnetic metamaterials are artificially engineered materials with characteristics tailored over a broad range of wavelengths.[4,5] Wavelength-selective narrow-band thermal emission control is a key technology with applications in high-efficiency thermophoto-voltaics,[6−8] incandescent light sources,[9] biosensing,[10−12] microbolometers,[13,14] imaging,[15] and infrared heaters.[16] Different types of artificial nanostructures have been proposed in the past few decades: multilayer,[17,18] photonic crystal,[19−21] and metal−insulator−metal (MIM) metamaterials.[22−27]

Development of metamaterial thermal radiators generally requires high-cost nanofabrication. The reported narrow-band thermal radiator with the highest Q-factor to date (∼200) consists of 2D-grating-coupled surface phonon polaritons.[28] However, there is still a problem because there are large unwanted peaks and background in the emissivity spectra in the target wavelength range. This can be quantified by the low value of the figure of merit (defined to evaluate the radiator performance as will be shown later) due to the low wavelength selectivity. In addition, including another experimental demonstration of multiple quantum wells and a photonic crystal slab with a Q-factor of 107,[29] the complicated fabrication process faces practical problems because many applications of radiators require large surface area. In this sense, among various classes of metamaterials, multilayers with relatively less complication in fabrication have merit in scalability. Control of thermal emission by multilayer structures has been successfully demonstrated with a Fabry−Perot resonator with a Q-factor of 87[30] and a distributed Bragg
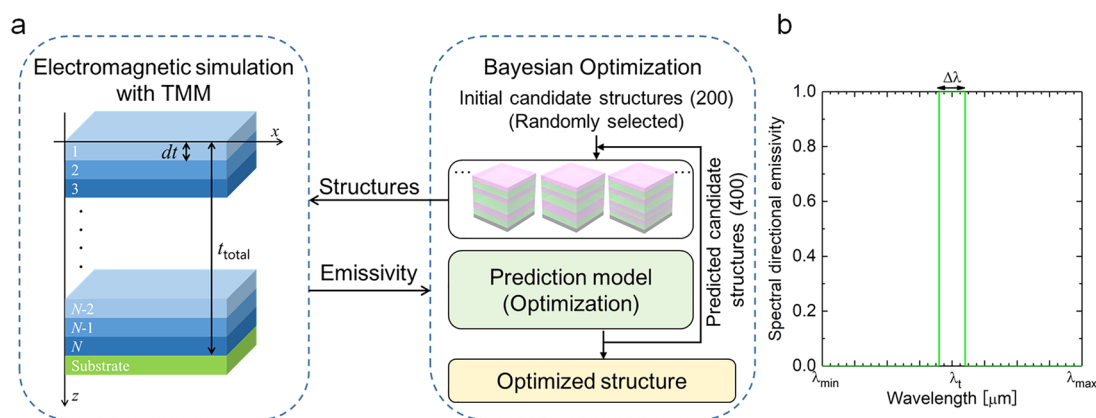
Figure 1. (a) Schematic of the optimization method with material informatics combining electromagnetic simulation and Bayesian optimization. (b) Schematic of the ideal optical property of the narrow-band thermal radiator.

reflector with a Q-factor of 36.[31] However, these structures are usually realized by simple and periodic design, despite the fact that periodic structures are a tiny subset of the entire possible range of multilayer structures. Several studies have reported control of light by such "aperiodic" multilayer structures,[32−36] but these results were obtained by numerical simulation. Furthermore, the optimal design of aperiodic multilayered metamaterials with desired thermal emission characteristics has been difficult because the search space, i.e., the number of possible candidates, becomes enormous.

The key technology to overcome this challenge is "materials informatics" (MI), which has the capability to efficiently identify materials with preferred properties. MI aims to identify the "best" materials with optimal structure and/or composition using unrecognized complex correlations in the data. It has been applied to find novel materials such as cathode materials for the lithium-ion batteries,[37] nitride semiconductors composed of earth-abundant materials,[38] piezoelectric materials,[39] and thermoelectric materials.[40−44] While these works have aimed to realize high-throughput screening of the best materials from the pool of stoichiometric compounds, another course of MI aims to create nanostructures by identifying the optimal geometry that maximizes the objective properties. This includes nanoparticles embedded in a matrix to modulate heat conduction,[45] solid−solid interfaces to identify energetically stable structures,[46] and multicore structures of plasmonic nanowires to control optical scattering and cloaking effects.[47]

On the basis of the above progress in geometry optimization, the methodology using Bayesian optimization has been extended to the design of nanostructures with optimal thermal conductance[48] and thermoelectric figure of merit.[49] There, to efficiently identify the optimal structures among the enormous number of candidates, phonon/electron transport calculations and machine learning/prediction are alternately conducted. The previous works have shown that such an approach can considerably accelerate nanostructure design for transport properties. As the method is not limited to phonons/electrons and is applicable to any other quasi-particles, this work aims to perform such optimization for polaritons and associated thermal radiation. It should be noted that for thermal radiation there have been reports on the optimal design of multilayer structures using a genetic algorithm,[50,51] but genetic algorithms do not involve machine learning/prediction. In addition, recent studies[52,53] reported numerical nanophotonics designs based on neural networks. The essential drawback of their

approach is that it is "exploitation-only". There is plenty of evidence that the exploitation-only approach cannot be more efficient than the approach balancing exploitation and exploration.[54] On the other hand, Bayesian optimization identifies an unknown function with respect to the descriptors with as few iterations as possible, where, at every iteration, learning and prediction based on a Gaussian process are performed. Our approach uses Bayesian inference to quantify uncertainties and takes the optimal balance between exploration and exploitation, and we have used it to solve an essentially more difficult problem than the ones solved using neural networks. Although the previous studies optimized the thickness of each layer only, we optimized how the three materials are arranged, i.e., our method optimizes the ordering of the materials as well. There are a huge number of possible orderings, which adds substantial difficulty to the optimization problem.

In this work, we computationally designed an ultranarrow-band wavelength-selective thermal radiator via Bayesian optimization methods[55] and experimentally demonstrated the optical characteristics of the designed multilayered metamaterials. Potential applications of this study include infrared sensors, infrared imaging, and infrared heaters since the target wavelength is in the mid-infrared range.

■ RESULTS AND DISCUSSION

Figure 1a shows a schematic of the optimization method with MI combining electromagnetic simulation and Bayesian optimization. The designed metamaterial is divided into N unit layers with thickness dt. A unit layer can be either Ge, Si, or SiO_2. The choice of compositions are commonly used semiconductor and dielectric materials for their high and low refractive indices, respectively. Since tungsten was chosen as the substrate, the substrate was considered opaque. Four basic elements are required when materials informatics is performed: the descriptor, calculator, evaluator, and optimization method. The descriptors are used to describe possible structure candidates during the optimization process. In this study, we used a text flag to indicate the state of each layer: "1", "2", and "3" represent the Ge, Si, and SiO_2 layers, respectively. Such a simple descriptor has been shown to realize efficient optimization[48,49] in addition to being intuitive, general, and practical, which are important in the actual material development. As for the calculator, we employed the transfer matrix

method (TMM) to calculate the emissivity spectra (see Methods).

The desired optical property of the ultranarrow-band thermal radiator is shown in Figure 1b. The ideal radiator has a sharp and high thermal emission at a target wavelength λ_t with a bandwidth $\Delta\lambda$, and low thermal emission in the rest of the infrared wavelength region to reduce radiative heat loss. For the evaluator of designed multilayered metasurfaces, a figure of merit (FOM) is defined as follows:

$$\text{FOM} = \frac{\int_{\lambda_t-\Delta\lambda/2}^{\lambda_t+\Delta\lambda/2} \varepsilon_\lambda I_{b\lambda} \, d\lambda}{\int_{\lambda_t-\Delta\lambda/2}^{\lambda_t+\Delta\lambda/2} I_{b\lambda} \, d\lambda} - \frac{\int_{\lambda_{min}}^{\lambda_t-\Delta\lambda/2} \varepsilon_\lambda I_{b\lambda} \, d\lambda}{\int_{\lambda_{min}}^{\lambda_t-\Delta\lambda/2} I_{b\lambda} \, d\lambda}$$

$$- \frac{\int_{\lambda_t+\Delta\lambda/2}^{\lambda_{max}} \varepsilon_\lambda I_{b\lambda} \, d\lambda}{\int_{\lambda_t+\Delta\lambda/2}^{\lambda_{max}} I_{b\lambda} \, d\lambda} \tag{1}$$

where ε_λ is the spectral normal emissivity, $I_{b\lambda}$ is the spectral blackbody intensity, and λ_{min} and λ_{max} are the minimum and maximum wavelengths considered for the optimization.

As we have N unit layers and three possible materials (Ge, Si, or SiO_2), the total number of candidate structures is 3^N, which becomes enormous for a useful range of N. For these large-scale problems, efficiency of optimization becomes critical, and thus, we need a method that surpasses conventional optimization tools. For this, we employ Bayesian optimization using the open-source library COMBO (see section S1 in the Supporting Information).

As shown in Figure 1a, suppose that FOMs of n candidates are initially calculated, and we are to select the next ones to calculate. A Bayesian regression function is learned from n pairs of descriptors and FOMs (i.e., training examples). For all of the remaining candidates, a predictive distribution of FOMs is estimated. Finally, FOMs are calculated for the selected candidates, and they are added to the training examples. By repetition of this procedure, the calculation of FOMs is scheduled optimally, and the optimized structure can be found quickly. Here, one problem is that the Bayesian optimization requires large computational memory because it uses information on the text data for all of the candidates. Therefore, we employed a hierarchical method to reduce the required size of computational memory, as will be explained later (also see Figure S1).

First, we computationally designed narrow-band thermal radiators with three candidate materials (Ge, Si, and SiO_2) for a target wavelength λ_t of 6.0 μm. The wavelengths $\Delta\lambda$, λ_{min}, and λ_{max} were set to 4 nm, 4 μm, and 8 μm, respectively. The number of layers N was fixed at 18. Variation of the total thicknesses of the multilayers, t_{total}, was also considered within the range from 3.6 to 4.0 μm with an increment of 0.02 μm, giving 21 variations of t_{total}. Therefore, the total number of possible candidates is $3^{18} \times 21 = 8\,135\,830\,269$. It should be noted that it was not possible to account for structures with translational and reversal symmetries prior to the calculation to reduce the number of candidates. In this case, the numbers of initial and predicted candidate structures were set to 200 and 400, respectively. The computational load for this calculation was so large that all of the candidates could not be evaluated. For the sake of saving the computational memory, the optimization was pursued in hierarchical steps; the overall candidates were randomly divided into 42 000 groups, and the optimization was first performed for each group, after which

the global best structure was identified by ranking these 42 000 local best structures. The total computational time was about 24 days on our cluster machine with 24 parallel computation (UNI-i9X, TOWA Electric, Inc.). The computational memory size in this work was about 128 GB, which set the maximum total number of layers to be 18. This could be enlarged by using a computer with a larger memory, but as the FOM of the designed structure is already close to unity, there is in fact not much room left for noticeable improvement even if we further increased the number of layers. Therefore, one can see the current setup to be nearly optimal and free from hardware restrictions.

The resulting optimized structures are shown in Figure 2a. It is interesting to note that the optimized structure with the
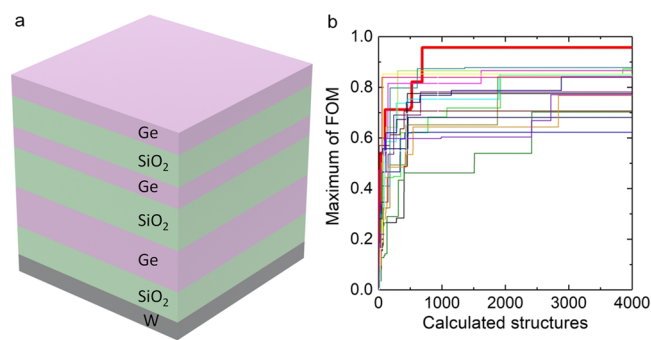

Figure 2. (a) Optimized structure of the narrow-band thermal emitter with three material candidates (Ge, Si, and SiO_2). The optimal structure turned out to consist of only Ge and SiO_2 layers. (b) Histories of the FOMs of 20 randomly selected groups. The global-maximum FOM was found in a certain group that is indicated by the thick red line.

maximum FOM consists of only Ge and SiO_2 layers despite the fact that the optimization was performed including Si also. The obtained structure is a counterintuitive aperiodic multilayer, which is explicitly different from conventional multilayered thermal radiators with periodic structures. The total thickness t_{total} of the optimal multilayer in this case is 3.80 μm.

Figure 2b shows the history of the maximum FOM with respect to the number of calculated structures. Here we randomly chose the cases of 20 groups with about 200 000 candidates each to show the optimization efficiency and its statistics. The maximum FOM could be realized within calculations of 168 000 000 structures on average, which means only 2.06% of the candidate structures needed to be calculated to identify the optimal structure.

We also designed two other types of narrow-band thermal radiators with different target wavelengths of 5.0 and 7.0 μm. For these cases, using the finding in the case of $\lambda_t = 6.0 \mu$m that the optimal structure consists only of two species (Ge and SiO_2), the optimization was performed for these two species instead of the above three species, which reduced the number of candidates to $2^{18} \times 21 = 5\,505\,024$. The bandwidth $\Delta\lambda$ (=4 nm) and the evaluation range of wavelengths ($\lambda_{min} = 4.0 \mu$m and $\lambda_{max} = 8.0 \mu$m) were kept the same as in the three-species optimization, and the number of initial candidate structures and predicted candidate structures were reduced to 100 and 20, respectively. The resulting optimized structures for $\lambda_t = 5.0$ and 7.0 μm (Figure 3a,b) consist of aperiodic multilayers similar to that for $\lambda_t = 6.0 \mu$m. The total thicknesses of the
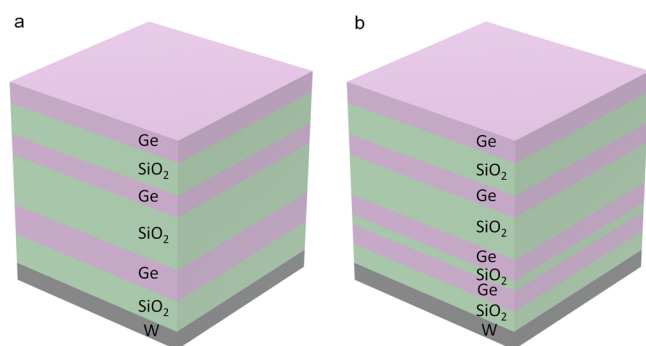
Figure 3. Optimized structures of the narrow-band thermal emitters for the target wavelengths of (a) 5.0 and (b) 7.0 μm.

multilayers for the corresponding samples are t_{total} = 3.78 and 3.96 μm, respectively.

The computational load for the two-species calculations was relatively small, so all of the candidates could be calculated to validate the optimal structure and efficiency. As a result, the optimal structures obtained by Bayesian optimization were confirmed to be exactly the same as the structures with maximum FOM among all of the candidates. We also confirmed from the probability distributions (see Figure S2) that the probability monotonically decreases as the FOM value approaches the maximum without noticeable local minima, indicating that the current problem is suited for Bayesian optimization.

Figure 4a shows the corresponding calculated spectral directional emissivities of the optimized structures. Extremely sharp and high emissivity can be realized with the optimized structures, and there are no extra peaks within the wavelength range of interest (from 4 to 8 μm). The corresponding emissivities of the peaks are unity, and their Q-factors are 217, 273, and 233 for λ_t = 5, 6, and 7 μm, respectively.

Finally, we experimentally fabricated the optimized structures by sputtering to demonstrate the feasibility of the structural optimization. Figure 4b shows the measured spectral directional emissivities of the fabricated structures. The three sharp peaks that correspond to the ones seen in the numerical simulations can be clearly observed, although the locations of the peaks are shifted by about 0.5 μm relative to the designed structures. The obtained peak emissivity values of the λ_t = 5, 6, and 7 μm samples are 0.76, 0.83, and 0.61, and the Q-factors are 132, 188, and 109, respectively. The reason for the

discrepancies in the peak positions and emissivities/Q-factors of the designed and fabricated structures could be that the thicknesses of the constituent layers in the fabricated samples somewhat deviate from the designed values. Table 1 quantifies

Table 1. Layer Thicknesses of the Designed and Fabricated Structures (in μm)

layer no.	λ_t = 5.0 μm		λ_t = 6.0 μm		λ_t = 7.0 μm	
	sim.	exp.	sim.	exp.	sim.	exp.
1	0.42	0.42	0.42	0.43	0.44	0.44
2	0.63	0.61	0.63	0.69	0.66	0.62
3	0.42	0.43	0.42	0.45	0.44	0.44
4	1.05	0.97	0.85	0.91	0.88	0.84
5	0.63	0.63	0.85	0.87	0.44	0.45
6	0.63	0.58	0.63	0.65	0.22	0.22
7	–	–	–	–	0.44	0.44
8	–	–	–	–	0.44	0.41

the moderate but non-negligible differences between the layer thicknesses of the designed and fabricated structures obtained from the cross-sectional transmission electron microscopy (TEM) image for λ_t = 6.0 μm (Figure 4c) and the cross-sectional scanning electron microscopy (SEM) images for λ_t = 5.0 μm and λ_t = 7.0 μm (Figure S3). When we calculated the spectral directional emissivity for the layer thicknesses in the fabricated sample (Table 1), the position of the peak approached the experimentally measured value (Figure S4). The remaining discrepancy can be attributed to the minor differences in the optical properties of the sputtered material and those used as inputs to the numerical simulation, since the optical properties may differ depending on fabrication conditions such as the deposition rate.

To determine the sharpness of the interface, the atomic concentrations at the Ge−SiO$_2$ interface were observed by energy-dispersive X-ray spectroscopy (EDX) (Figures S5 and S6), and the interface was confirmed to be sharp with small interdiffusion. Although fabrication with a more accurately calibrated sputtering process would improve the reproduction of the designed performance, which remains to be our future task, the key features in the designed structure, namely, ultranarrow-band emission with controlled peak wavelength, were clearly realized in the experiments. The obtained Q-factors are about 217−273 in the computational design and about 109−188 in the experiment, which are significantly
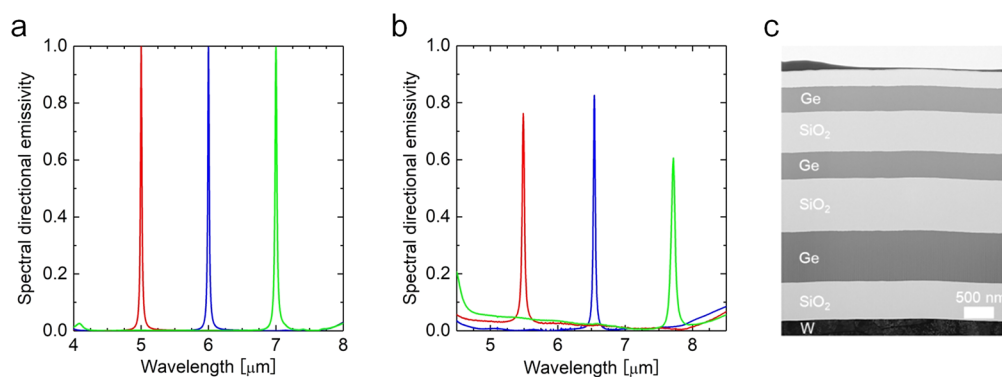

Figure 4. (a) Calculated spectral directional emissivities of the optimized structures obtained with Bayesian optimization and (b) measured spectral directional emissivities of the fabricated structures aimed at λ_t = 5.0 μm (red), 6.0 μm (blue), and 7.0 μm (green). (c) Cross-sectional TEM images of the fabricated sample for λ_t = 6.0 μm.
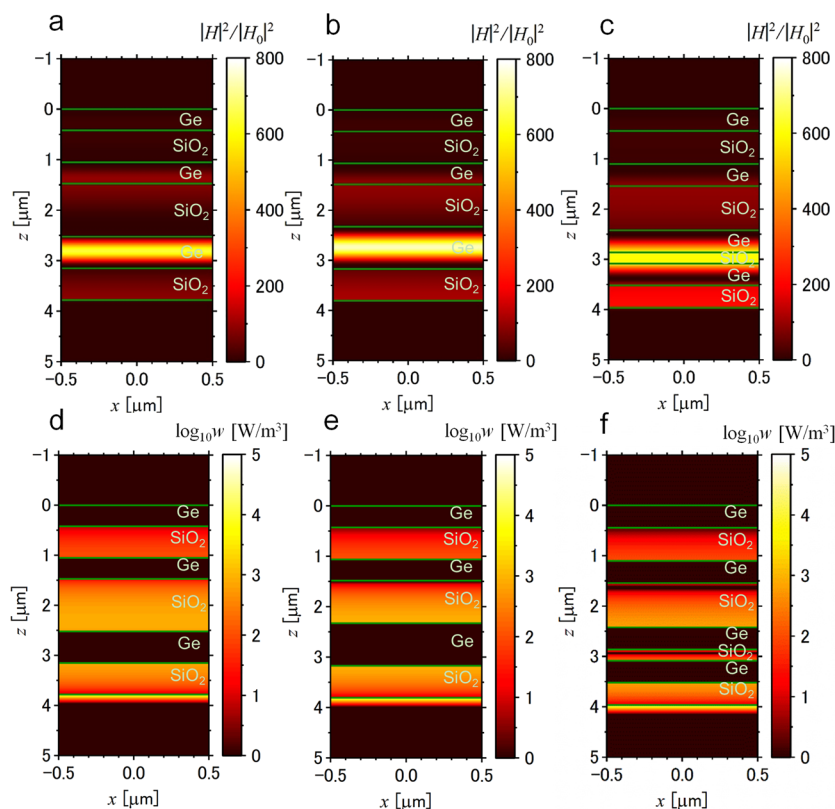
Figure 5. (a−c) Contour plots of normalized magnetic field intensity and (d−f) power dissipation density for target wavelengths of (a, d) 5.0 μm, (b, e) 6.0 μm, and (c, f) 7.0 μm.

higher than the values reported in the previous studies. In addition, the FOM of this work is significantly higher than in previous experimental work:[28] the FOM of previous work, evaluated with the same wavelength range around the target wavelengths, was only 0.02 for 0° and further decreased to −0.16 for 1°, which are considerably smaller than the FOM of 0.77 for the current structure aimed at 6 μm. Although the locally extracted Q-factor in the previous work reached 200,[28] the emissivity spectra had much larger background and unwanted peaks, and thus, our experiment exhibits significantly higher wavelength selectivity. To our knowledge, this is the first demonstration that narrow-band thermal radiators designed by machine learning can be realized in experiments.

We now discuss the mechanism of the enhanced emission in terms of the magnetic field profiles shown in Figure 5. The intensities of the magnetic profiles were normalized by the intensity of the normal incident light. In Figure 5a,b for λ_t = 5 and 6 μm, there are strong confinements of electromagnetic energy in the Ge layer. On the other hand, in Figure 5c, for λ_t = 7 μm, strong confinement can be observed in the SiO$_2$ layer. These emissivity enhancements originate from localized modes, similar to defect modes of photonic crystals.[56] Defect modes of photonic crystals exist inside a photonic band gap; therefore, this phenomenon is usually observed with periodic structures (see section S3). However, it is interesting to note that we observed a similar localized mode inside the aperiodic multilayered metamaterials. In other words, two or more optimized defect layers are introduced into the photonic crystals that effectively serve to constitute a sharp peak in the emissivity. In particular, in Figure 5c, the defect layer corresponds to three layers of a thin SiO$_2$ layer and upper and lower Ge layers sandwiching the SiO$_2$ layer. Therefore, the

aperiodic structure, when optimized, successfully suppresses the unnecessary emissivity peaks due to higher-order harmonics, or in other words, shifts the peaks to a shorter wavelength range. To quantify how much power is absorbed by the proposed structure, the power dissipation density w was calculated as[57]

$$w = \frac{1}{2}\varepsilon_0\varepsilon''\omega\,|\mathbf{E}|^2 \tag{2}$$

where ε_0 is the permittivity of vacuum, ε'' is the imaginary part of the complex dielectric function, and ω is the angular frequency. The power dissipation densities, which are shown in Figure 5d−f, indicate the strong absorption at the tungsten substrate, although there is weak absorption within the SiO$_2$ layer. Therefore, thermal energy dissipation mainly occurs in the metallic substrate because of the large optical loss.

Because of the localized mode of the electromagnetic wave, the proposed emitter has an angular dependence of the optical properties (Figure S8). Isotropic thermal emission is preferred in certain applications such as infrared heaters. In this design, the angular dependences of the optical properties of transverse magnetic and transverse electric polarization within 20° are small, as the spectral shifts were only about 1%, which therefore is acceptable for practical applications. It should be noted that it is also possible to include the angular dependence in the FOM for preferred angular dependence, which will be explored in the future. The obtained results enhance our understanding of the narrow-band thermal emission mechanism of aperiodic multilayered metamaterials and facilitate the effective design of new metamaterials via Bayesian optimization.

CONCLUSION

We computationally designed ultranarrow-band wavelength-selective thermal radiators via Bayesian optimization methods and experimentally demonstrated the optical characteristics of the designed multilayered metamaterials. The optimized structures could be found within calculations of only a few percent of the total numbers of candidate structures. The optimized structure for each target wavelength consists of aperiodic multilayers that give rise to sharp and near-unity emissivity. The designed structures were experimentally realized with reasonable accuracy, and the obtained structures exhibit Q-factors significantly larger than in previous works based on empirical design. Post-analysis of the magnetic fields of the structures revealed that the aperiodic multilayers can result in highly effective localization. The current work demonstrates the effectiveness, feasibility, and accuracy of developing narrow-band thermal emission materials using Bayesian optimization. In addition, the follow-up analysis of the mechanism demonstrates that such a materials informatics approach is also useful to enhance our understanding of narrow-band thermal emission.

METHODS

Safety Statement. No unexpected or unusually high safety hazards were encountered.

Electromagnetic Simulation. The TMM was used to solve Maxwell's equations, allowing the calculation of the spectral radiative properties of multilayered metamaterials.[58] The spectral directional emissivity could be obtained by applying Kirchhoff's law, i.e., $\varepsilon_\lambda = 1 - R_\lambda$, where R_λ is the reflectance obtained from the TMM simulation. The dielectric functions of SiO_2, Si, Ge, and W were obtained from tabulated data.[59]

Bayesian Optimization. Bayesian optimization is a design algorithm based on machine learning[60] and a well-established technique for black-box optimization.[55] Bayesian prediction models are employed to predict the black-box function, where the uncertainty of the predicted function is also evaluated as predictive variance. The next candidate for the experiment is selected on the basis of predicted values and variances. Bayesian optimization has been recognized as an important technique in machine learning research because of successful hyperparameter tuning in deep learning algorithms. Bayesian optimization can be applied not only to materials sciences but also to various kinds of problems. However, the precondition is that each candidate point is represented as a numerical vector of identical dimensionality (i.e., descriptor).

Sample Fabrication and Reflectivity Measurement. The narrow-band thermal radiators designed on the basis of the Bayesian optimization method were experimentally fabricated and characterized. SiO_2 and Ge layers were alternately deposited on a tungsten substrate by a magnetron sputtering machine. An FTIR spectrometer (iS50R, Thermo Scientific Nicolet) was used for reflectivity measurements, with an opaque gold film as a reference. In order to avoid atmospheric absorption, the measurements were conducted with flowing nitrogen gas. The incident angle was arranged within 1°, and therefore, the measured spectral reflectivity data could be considered as near normal reflectivity. Once the reflectivity was obtained, the spectral directional emissivity was obtained by applying Kirchhoff's law.

ASSOCIATED CONTENT

Ⓢ Supporting Information

The Supporting Information is available free of charge on the ACS Publications website at DOI: 10.1021/acscentsci.8b00802.

> Bayesian optimization, visualization and analysis of the nanostructure, and photonic band gap and localized mode (PDF)

AUTHOR INFORMATION

Corresponding Author

*E-mail: shiomi@photon.t.u-tokyo.ac.jp.

ORCID Ⓞ

Shenghong Ju: 0000-0001-7863-6947
Tadaaki Nagao: 0000-0002-6746-2686
Koji Tsuda: 0000-0002-4288-1606
Junichiro Shiomi: 0000-0002-3552-4555

Author Contributions

A.S., K.Y., T.S, S.J, H.O., K.T., and J.S. contributed to the computational design; M.K. and J.S. contributed to the structure fabrication; T.N. contributed to the emissivity measurements; A.S. and J.S. designed the project and wrote the paper. All of the authors reviewed the manuscript.

Notes

The authors declare no competing financial interest.

REFERENCES

(1) Fan, S. Thermal photonics and energy applications. *Joule* **2017**, *1* (2), 264−273.

(2) Cui, L. J.; Jeong, W.; Fernandez-Hurtado, C.; Feist, J.; Garcia-Vidal, F. J.; Cuevas, J. C.; Meyhofer, E.; Reddy, P. Study of radiative heat transfer in Angstrom- and nanometre-sized gaps. *Nat. Commun.* **2017**, *8*, 14479.

(3) Gluchko, S.; Palpant, B.; Volz, S.; Braive, R.; Antoni, T. Thermal excitation of broadband and long-range surface waves on SiO2 submicron films. *Appl. Phys. Lett.* **2017**, *110* (26), 263108.

(4) Pendry, J. B.; Holden, A. J.; Robbins, D. J.; Stewart, W. J. Magnetism from conductors and enhanced nonlinear phenomena. *IEEE Trans. Microwave Theory Tech.* **1999**, *47* (11), 2075−2084.

(5) Smith, D. R.; Pendry, J. B.; Wiltshire, M. C. K. Metamaterials and negative refractive index. *Science* **2004**, *305* (5685), 788−792.

(6) De Zoysa, M.; Asano, T.; Mochizuki, K.; Oskooi, A.; Inoue, T.; Noda, S. Conversion of broadband to narrowband thermal emission through energy recycling. *Nat. Photonics* **2012**, *6* (8), 535−539.

(7) Bierman, D. M.; Lenert, A.; Chan, W. R.; Bhatia, B.; Celanovic, I.; Soljacic, M.; Wang, E. N. Enhanced photovoltaic energy conversion using thermally based spectral shaping. *Nat. Energy* **2016**, *1*, 16068.

(8) Zhou, Z.; Yehia, O.; Bermel, P. Integrated photonic crystal selective emitter for thermophotovoltaics. *J. Nanophotonics* **2016**, *10*, No. 016014.

(9) Ilic, O.; Bermel, P.; Chen, G.; Joannopoulos, J. D.; Celanovic, I.; Soljacic, M. Tailoring high-temperature radiation and the resurrection of the incandescent source. *Nat. Nanotechnol.* **2016**, *11* (4), 320−324.

(10) Liu, N.; Mesch, M.; Weiss, T.; Hentschel, M.; Giessen, H. Infrared perfect absorber and its application as plasmonic sensor. *Nano Lett.* **2010**, *10* (7), 2342−2348.

(11) Wu, C. H.; Khanikaev, A. B.; Adato, R.; Arju, N.; Yanik, A. A.; Altug, H.; Shvets, G. Fano-resonant asymmetric metamaterials for ultrasensitive spectroscopy and identification of molecular monolayers. *Nat. Mater.* **2012**, *11* (1), 69−75.

(12) Luo, S.; Zhao, J.; Zuo, D.; Wang, X. Perfect narrow band absorber for sensing applications. *Opt. Express* **2016**, *24* (9), 9288−9294.

(13) Liu, X. L.; Wang, L. P.; Zhang, Z. M. Wideband tunable omnidirectional infrared absorbers based on doped-silicon nanowire arrays. *J. Heat Transfer* **2013**, *135* (6), No. 061602.

(14) Du, K.; Li, Q.; Zhang, W.; Yang, Y.; Qiu, M. Wavelength and thermal distribution selectable microbolometers based on metamaterial absorbers. *IEEE Photonics J.* **2015**, *7* (3), 1−8.

(15) Landy, N. I.; Bingham, C. M.; Tyler, T.; Jokerst, N.; Smith, D. R.; Padilla, W. J. Design, theory, and measurement of a polarization-insensitive absorber for terahertz imaging. *Phys. Rev. B: Condens. Matter Mater. Phys.* **2009**, *79* (12), 125104.

(16) Totani, T.; Sakurai, A.; Kondo, Y. A wavelength control emitter for drying furnace. In *Proceedings of the Asian Conference on Thermal Sciences 2017*; KSME: Seoul, Korea, 2017; Paper ACTS-P00423.

(17) Bermel, P.; Ghebrebrhan, M.; Chan, W.; Yeng, Y. X.; Araghchini, M.; Hamam, R.; Marton, C. H.; Jensen, K. F.; Soljacic, M.; Joannopoulos, J. D.; Johnson, S. G.; Celanovic, I. Design and global optimization of high-efficiency thermophotovoltaic systems. *Opt. Express* **2010**, *18* (19), A314−A334.

(18) Wang, H.; Alshehri, H.; Su, H.; Wang, L. Design, fabrication and optical characterizations of large-area lithography-free ultrathin multilayer selective solar coatings with excellent thermal stability in air. *Sol. Energy Mater. Sol. Cells* **2018**, *174*, 445−452.

(19) Nam, Y.; Yeng, Y. X.; Lenert, A.; Bermel, P.; Celanovic, I.; Soljacic, M.; Wang, E. N. Solar thermophotovoltaic energy conversion systems with two-dimensional tantalum photonic crystal absorbers and emitters. *Sol. Energy Mater. Sol. Cells* **2014**, *122*, 287−296.

(20) Rinnerbauer, V.; Lenert, A.; Bierman, D. M.; Yeng, Y. X.; Chan, W. R.; Geil, R. D.; Senkevich, J. J.; Joannopoulos, J. D.; Wang, E. N.; Soljacic, M.; Celanovic, I. Metallic photonic crystal absorber-emitter for efficient spectral control in high-temperature solar thermophotovoltaics. *Adv. Energy Mater.* **2014**, *4* (12), 1400334.

(21) Yeng, Y. X.; Chou, J. B.; Rinnerbauer, V.; Shen, Y.; Kim, S.-G.; Joannopoulos, J. D.; Soljacic, M.; Celanovic, I. Global optimization of omnidirectional wavelength selective emitters/absorbers based on dielectric-filled anti-reflection coated two-dimensional metallic photonic crystals. *Opt. Express* **2014**, *22* (18), 21711−21718.

(22) Landy, N. I.; Sajuyigbe, S.; Mock, J. J.; Smith, D. R.; Padilla, W. J. Perfect metamaterial absorber. *Phys. Rev. Lett.* **2008**, *100* (20), 207402.

(23) Aydin, K.; Ferry, V. E.; Briggs, R. M.; Atwater, H. A. Broadband polarization-independent resonant light absorption using ultrathin plasmonic super absorbers. *Nat. Commun.* **2011**, *2*, 517.

(24) Sakurai, A.; Zhao, B.; Zhang, Z. M. Resonant frequency and bandwidth of metamaterial emitters and absorbers predicted by an RLC circuit model. *J. Quant. Spectrosc. Radiat. Transfer* **2014**, *149*, 33−40.

(25) Sakurai, A.; Zhao, B.; Zhang, Z. M. Effect of polarization on dual-band infrared metamaterial emitters or absorbers. *J. Quant. Spectrosc. Radiat. Transfer* **2015**, *158*, 111−118.

(26) Dao, T. D.; Ishii, S.; Yokoyama, T.; Sawada, T.; Sugavaneshwar, R. P.; Chen, K.; Wada, Y.; Nabatame, T.; Nagao, T. Hole array perfect absorbers for spectrally selective mid-wavelength infrared pyroelectric detectors. *ACS Photonics* **2016**, *3* (7), 1271−1278.

(27) Matsuno, Y.; Sakurai, A. Perfect infrared absorber and emitter based on a large-area metasurface. *Opt. Mater. Express* **2017**, *7* (2), 618−626.

(28) Dahan, N.; Niv, A.; Biener, G.; Gorodetski, Y.; Kleiner, V.; Hasman, E. Extraordinary coherent thermal emission from SiC due to coupled resonant cavities. *J. Heat Transfer* **2008**, *130* (11), 112401.

(29) Inoue, T.; De Zoysa, M.; Asano, T.; Noda, S. Single-peak narrow-bandwidth mid-infrared thermal emitters based on quantum wells and photonic crystals. *Appl. Phys. Lett.* **2013**, *102* (19), 191110.

(30) Zhao, D.; Meng, L.; Gong, H.; Chen, X.; Chen, Y.; Yan, M.; Li, Q.; Qiu, M. Ultra-narrow-band light dissipation by a stack of lamellar silver and alumina. *Appl. Phys. Lett.* **2014**, *104* (22), 221107.

(31) Yang, Z.-Y.; Ishii, S.; Yokoyama, T.; Dao, T. D.; Sun, M.-G.; Pankin, P. S.; Timofeev, I. V.; Nagao, T.; Chen, K.-P. Narrowband wavelength selective thermal emitters by confined tamm plasmon polaritons. *ACS Photonics* **2017**, *4* (9), 2212−2219.

(32) Granier, C. H.; Afzal, F. O.; Min, C.; Dowling, J. P.; Veronis, G. Optimized aperiodic highly directional narrowband infrared emitters. *J. Opt. Soc. Am. B* **2014**, *31* (6), 1316−1321.

(33) Sahel, S.; Amri, R.; Gamra, D.; Lejeune, M.; Benlahsen, M.; Zellama, K.; Bouchriha, H. Effect of sequence built on photonic band gap properties of one-dimensional quasi-periodic photonic crystals: application to thue-morse and double-period structures. *Superlattices Microstruct.* **2017**, *111*, 1−9.

(34) Rephaeli, E.; Fan, S. Absorber and emitter for solar thermophotovoltaic systems to achieve efficiency exceeding the Shockley-Queisser limit. *Opt. Express* **2009**, *17* (17), 15145−15159.

(35) Drevillon, J.; Ben-Abdallah, P. Ab initio design of coherent thermal sources. *J. Appl. Phys.* **2007**, *102* (11), 114305.

(36) Sergeant, N. P.; Pincon, O.; Agrawal, M.; Peumans, P. Design of wide-angle solar-selective absorbers using aperiodic metal-dielectric stacks. *Opt. Express* **2009**, *17* (25), 22800−22812.

(37) Nishijima, M.; Ootani, T.; Kamimura, Y.; Sueki, T.; Esaki, S.; Murai, S.; Fujita, K.; Tanaka, K.; Ohira, K.; Koyama, Y.; Tanaka, I. Accelerated discovery of cathode materials with prolonged cycle life for lithium-ion battery. *Nat. Commun.* **2014**, *5*, 4553.

(38) Hinuma, Y.; Hatakeyama, T.; Kumagai, Y.; Burton, L. A.; Sato, H.; Muraba, Y.; Iimura, S.; Hiramatsu, H.; Tanaka, I.; Hosono, H.; Oba, F. Discovery of earth-abundant nitride semiconductors by computational screening and high-pressure synthesis. *Nat. Commun.* **2016**, *7*, 11962.

(39) Xue, D.; Balachandran, P. V.; Yuan, R.; Hu, T.; Qian, X.; Dougherty, E. R.; Lookman, T. Accelerated search for BaTiO3-based piezoelectrics with vertical morphotropic phase boundary using Bayesian learning. *Proc. Natl. Acad. Sci. U. S. A.* **2016**, *113* (47), 13301−13306.

(40) Carrete, J.; Li, W.; Mingo, N.; Wang, S.; Curtarolo, S. Finding unprecedentedly low-thermal-conductivity half-Heusler semiconductors via high-throughput materials modeling. *Phys. Rev. X* **2014**, *4* (1), No. 011019.

(41) Seko, A.; Togo, A.; Hayashi, H.; Tsuda, K.; Chaput, L.; Tanaka, I. Prediction of low-thermal-conductivity compounds with first-principles anharmonic lattice-dynamics calculations and Bayesian optimization. *Phys. Rev. Lett.* **2015**, *115* (20), 205901.

(42) Oliynyk, A. O.; Antono, E.; Sparks, T. D.; Ghadbeigi, L.; Gaultois, M. W.; Meredig, B.; Mar, A. High-throughput machine-learning-driven synthesis of full-heusler compounds. *Chem. Mater.* **2016**, *28* (20), 7324−7331.

(43) van Roekeghem, A.; Carrete, J.; Oses, C.; Curtarolo, S.; Mingo, N. High-throughput computation of thermal conductivity of high-temperature solid phases: the case of oxide and fluoride perovskites. *Phys. Rev. X* **2016**, *6* (4), No. 041061.

(44) Gaultois, M. W.; Oliynyk, A. O.; Mar, A.; Sparks, T. D.; Mulholland, G. J.; Meredig, B. Perspective: Web-based machine learning models for real-time screening of thermoelectric materials properties. *APL Mater.* **2016**, *4* (5), No. 053213.

(45) Zhang, H.; Minnich, A. J. The best nanoparticle size distribution for minimum thermal conductivity. *Sci. Rep.* **2015**, *5*, 8995.

(46) Kiyohara, S.; Oda, H.; Tsuda, K.; Mizoguchi, T. Acceleration of stable interface structure searching using a kriging approach. *Jpn. J. Appl. Phys.* **2016**, *55* (4), No. 045502.

(47) Mirzaei, A.; Miroshnichenko, A. E.; Shadrivov, I. V.; Kivshar, Y. S. Superscattering of light optimized by a genetic algorithm. *Appl. Phys. Lett.* **2014**, *105* (1), No. 011109.

(48) Ju, S.; Shiga, T.; Feng, L.; Hou, Z.; Tsuda, K.; Shiomi, J. Designing nanostructures for phonon transport via Bayesian optimization. *Phys. Rev. X* **2017**, *7* (2), No. 021024.

(49) Yamawaki, M.; Ohnishi, M.; Ju, S.; Shiomi, J. Multifunctional structural design of graphene thermoelectrics by Bayesian optimization. *Sci. Adv.* **2018**, *4* (6), No. eaar4192.

(50) Shimazaki, K.; Ohnishi, A.; Nagasaka, Y. Development of spectral selective multilayer film for a variable emittance device and its radiation properties measurements. *Int. J. Thermophys.* **2003**, *24* (3), 757−769.

(51) Sakurai, A.; Tanikawa, H.; Yamada, M. Computational design for a wide-angle cermet-based solar selective absorber for high temperature applications. *J. Quant. Spectrosc. Radiat. Transfer* **2014**, *132*, 80−89.

(52) Peurifoy, J.; Shen, Y.; Jing, L.; Yang, Y.; Cano-Renteria, F.; DeLacy, B. G.; Joannopoulos, J. D.; Tegmark, M.; Soljacic, M. Nanophotonic particle simulation and inverse design using artificial neural networks. *Sci. Adv.* **2018**, *4* (6), No. eaar4206.

(53) Liu, D.; Tan, Y.; Khoram, E.; Yu, Z. Training deep neural networks for the inverse design of nanophotonic structures. *ACS Photonics* **2018**, *5* (4), 1365−1369.

(54) Shahriari, B.; Swersky, K.; Wang, Z.; Adams, R. P.; de Freitas, N. Taking the human out of the loop: a review of Bayesian optimization. *Proc. IEEE* **2016**, *104* (1), 148−175.

(55) Ueno, T.; Rhone, T. D.; Hou, Z.; Mizoguchi, T.; Tsuda, K. COMBO: An efficient Bayesian optimization library for materials science. *Materials Discovery* **2016**, *4*, 18−21.

(56) Joannopoulos, J. D.; Villeneuve, P. R.; Fan, S. Photonic crystals: putting a new twist on light. *Nature* **1997**, *386*, 143.

(57) Zhao, J. M.; Zhang, Z. M. Electromagnetic energy storage and power dissipation in nanostructures. *J. Quant. Spectrosc. Radiat. Transfer* **2015**, *151*, 49−57.

(58) Zhang, Z. M. *Nano/Microscale Heat Transfer*; McGraw-Hill: New York, 2007.

(59) Palik, E. D. *Handbook of Optical Constants of Solids*; Palik, E. D., Ed.; Academic Press: San Diego, CA, 1998; Vol. 3 .

(60) Dieb, T. M.; Tsuda, K. Machine Learning-Based Experimental Design in Materials Science. In *Nanoinformatics*; Tanaka, I., Ed.; Springer: Singapore, 2018; pp 65−74.